Turbulent stress at the ice/ocean interface and bottom surface hydraulic roughness during the SHEBA drift

Miles G. McPhee

McPhee Research Company, Naches, Washington, USA

Received 11 September 2000; revised 20 June 2001; accepted 5 November 2001; published 13 September 2002.

[1] Upper ocean turbulence and mean current data from the 1997–1998 Surface Heat Budget of the Arctic Ocean (SHEBA) drift in the western Arctic Ocean were used to estimate turbulent shear stress at the ice/ocean interface and hydraulic roughness of the ice undersurface. Techniques for determining interfacial stress from velocity covariance measurements in the ice/ocean boundary layer (IOBL) are complicated by buoyancy flux and the heterogeneity of the ice undersurface, where protrusions corresponding to relatively small upper surface features become major obstacles when compared to the scale of the IOBL. In addition, ice deformation forced relocation of the main SHEBA oceanographic program about midway through the experiment. Hence, there were two different measurement sites to consider. Three different methods were used to compute the undersurface roughness characterizing the undeformed, multiyear floe occupied by the SHEBA project. The first was straightforward (naive) application of the "law of the wall" to turbulent stress and mean velocity measurements from the turbulence instrument cluster nearest to the interface, assuming a logarithmic velocity profile and constant stress. For the second method, *local turbulence closure* was used to model the entire IOBL in order to estimate the impact of Coriolis stress attenuation and buoyancy forces on stress and shear near the boundary. A third method, proposed here for the first time, estimated mixing length and eddy viscosity from a scale inversely proportional to the wave number at the peak of the weighted vertical velocity spectrum. The last method appears most robust, in that it shows no overall difference in z_0 between the two sites and only minor seasonal and directional differences. The best estimate for the undersurface roughness of undeformed, multiyear ice at the SHEBA site is $0.0048\ \mathrm{m} < z_0 < 0.007$, i.e., about 6 mm. Specification of a regional "aggregate" under-ice roughness requires additional consideration of the added drag from isolated pressure keels and floe edges, along with reduced drag from smoother, newly frozen ice and open water. *INDEX TERMS:* 4207 Oceanography: General: Arctic and Antartic oceangoraphy; 4540 Oceanography: Physical: Ice mechanics and air/sea/ice exchange processes; 4568 Oceanography: Physical: Turbulence, diffusion, and mixing processes; 4572 Oceanography: Physical: Upper ocean processes; *KEYWORDS:* air-ice-ocean interaction, hydraulic roughness, ice-ocean stress, SHEBA

Citation: McPhee, M. G., Turbulent stress at the ice/ocean interface and bottom surface hydraulic roughness during the SHEBA drift, *J. Geophys. Res.*, *107*(C10), 8037, doi:10.1029/2000JC000633, 2002.

1. Introduction

[2] Estimates of under-ice drag coefficients and the undersurface roughness length (z_0) made from measurements in the ice/ocean boundary layer (IOBL) vary widely [e.g., *Untersteiner and Badgley*, 1965; *Ling and Untersteiner*, 1974; *Shirasawa*, 1986; *McPhee*, 1990], with z_0 ranging from hydraulically smooth under fast ice [*Crawford et al.*, 1999] through 1–2 mm for first-year ice in the Weddell Sea [*McPhee et al.*, 1999] to as high 6–7 cm in the marginal ice zone [*Pease et al.*, 1983; *McPhee et al.*, 1987]. With few exceptions, however, pack ice models and coupled ice/ocean models have in the past parameterized ice/ocean momentum flux with a constant quadratic drag coefficient: $u_{*0}\boldsymbol{u}_{*0} = \boldsymbol{c}_w U\boldsymbol{U}$, where $u_{*0}{}^2$ is the magnitude of kinematic (Reynolds) stress, $\boldsymbol{U}$ is ice velocity relative to some reference level in the ocean, and $\boldsymbol{c}_w = |\boldsymbol{c}_w|e^{i\beta}$ is a complex drag coefficient allowing for turning (β) of the stress traction vector relative to $\boldsymbol{U}$ (boldface type denotes a complex, two-dimensional vector). Ice models [e.g., *Hibler*, 1980; *Lemke et al.*, 1990; *Stössel*, 1992] have commonly assigned constant magnitude and turning (0.0055 and 25°) to $\boldsymbol{c}_w$, obtained from the free-drift force balance at the manned AIDJEX stations [*McPhee*, 1980]. That estimate was based on a comparatively high value (0.0027) for the 10-m surface wind drag coefficients, inferred by adjusting atmospheric turbulence mast measurements with the

0148-0227/02/2000JC000633$09.00

momentum integral calculated from pilot balloon profiles and inversion height [*Carsey*, 1980].

[3] There are several drawbacks to using a constant drag coefficient to calculate stress at the ice/ocean interface, which become increasingly apparent as resolution and physical sophistication of numerical models improve. First, a constant (neutral) drag coefficient is valid only if the reference level in the IOBL is within the *surface layer* where the turbulence scale depends mainly on distance from the interface (i.e., the mixing length is $\kappa|z|$) and the velocity profile is logarithmic. For the IOBL this holds only for the first few meters from the interface. Beyond the surface layer, turbulence scales with the planetary length scale, u_{*0}/f where f is the Coriolis parameter [e.g., *McPhee and Smith*, 1976; *McPhee and Martinson*, 1994]. In a similarity sense, this means that the nondimensional roughness of the surface (proportional to fz_0/u_{*0}) decreases with increasing stress, i.e., drag is velocity dependent. In addition, β (which is nonzero beyond the surface layer) decreases with increasing stress. If the reference level in the ocean is below the turbulent boundary layer (i.e., at a level where ocean flow is geostrophic), the effect of the planetary scaling may be expressed by Rossby similarity drag [e.g., *Blackadar and Tennekes*, 1968; *McPhee*, 1990]:

$$\Gamma = \boldsymbol{U}/\boldsymbol{u}_{*_0} = (1/\kappa)\Big(\log Ro_* - A - iB\Big) \qquad (1)$$

where here $\boldsymbol{U}$ is the complex ice velocity relative to undisturbed (geostrophic) flow in the ocean, κ is von Kàrmàn's constant (0.4), $Ro_* = |u_{*0}|/(fz_0)$ is the surface friction Rossby number, A and B are dimensionless scalar parameters that may depend on surface buoyancy flux (stability). The nondimensional surface velocity (inverse of geostrophic drag) varies as $-\log z_0$, which is the fundamental parameter for describing the under-ice roughness.

[4] In addition to rotation, buoyancy flux at the interface ($\langle w'b'\rangle_0$), which is typically proportional to the melting or freezing rate, [*McPhee*, 1990] may have a substantial impact on turbulence scales and ice/ocean drag. A common way of characterizing the effect of buoyancy is via the Obukhov length $L = {u_{*0}}^3/\kappa\langle w'b'\rangle_0$ [*Obukhov*, 1971]. Turbulence measurements in the IOBL suggest [*McPhee*, 1994] that in a horizontally homogeneous flow driven by shear (ice motion), turbulence is controlled mainly by the smallest of the three scales: $\kappa|z|$, κL, or $\Lambda_* u_{*0}/f$ where Λ_* is a similarity constant, about 0.03. While the functional form of the relationship between flow velocity and interfacial stress may be complicated, drag depends essentially on the ratio of the governing turbulence scale to z_0. In laboratory studies over uniformly rough surfaces, z_0 is found to be about 1/30 of the vertical extent of roughness elements. Adjacent to surfaces like the pack ice underside, with a broad spectrum of surface relief, no such simple relationship has been established.

[5] In a true "logarithmic surface layer" (i.e., current shear varies inversely with distance from a solid surface, variation in stress negligible), there is a direct relationship between a neutral drag coefficient defined at a particular level ($z = -h$) and roughness length:

$$c_w = \left(\frac{1}{\kappa}\log\frac{h}{z_0}\right)^{-2} \qquad h \text{ in the log layer} \qquad (2)$$

It would thus seem reasonable to confine measurements to the logarithmic surface layer in order to determine z_0, as is typically done in the atmosphere. The problem with this approach lies with the assumption of horizontal homogeneity. Multiyear pack ice in the interior Arctic Ocean often comprises floes of relatively undeformed ice with a fair amount of vertical relief on the underside from hummock and false bottom formation during summer. The floes are typically bordered in winter both by pressure ridges and smooth ice in frozen (or freezing) leads, and in summer by open leads. All may have very different impact on the overall drag affecting ice motion.

[6] A central issue in Surface Heat Budget of the Arctic Ocean (SHEBA) is "scaling up" from measurements made in the vicinity of the main SHEBA station to an area representative of a grid cell for large scale numerical models. For the ice undersurface, this is a formidable problem. Consider, for example, the impact of an isolated pressure ridge. For the atmosphere, a 2-m sail would typically represent less than 1% of the total atmospheric boundary layer (ABL) extent. The sail would be isostatically balanced by a keel extending down 10–15 m, constituting half or more of the typical IOBL extent observed during SHEBA. A midlatitude atmospheric analog would be a 500-m high hill protruding from the surrounding terrain. Similarly, at frozen lead edges, the surface roughness may change abruptly from a typical pack ice value of about a centimeter, to hydraulically smooth (0.02 mm would be a typical equivalent roughness) in a horizontal span of a few meters, further complicated by the possibility of flow separation and intense turbulence at the step change in thickness.

[7] The strategy adopted for the SHEBA ocean turbulence program was to deploy the main mast under ice considered typical, and continue measuring at the central location in order to characterize that surface. Over the course of the year, there would be flow from all different directions with different upstream conditions. A series of shorter special intensive observing periods (IOPs) was planned, with deployments to measure IOBL turbulence near pressure ridge keels, under thin ice, and near summer leads. The IOP data would be combined with sophisticated modeling to gauge the influence of such features on the overall momentum exchange. These effects could then be estimated for different ice type concentrations (remotely sensed), and their impact added in some weighted fashion to momentum transfer of undeformed ice. A central tenet of this strategy is that there is some underlying roughness length characterizing a multiyear, undeformed ice floe. Over the course of the yearlong SHEBA experiment, we did encounter flow from all directions (including directly across upstream pressure ridge keels) and a wide range of U/u_{*0} ratios, even at the uppermost measurement level. We were also forced to relocate the measurement site about halfway through the experiment. A valid question is whether there is too much variability in the undersurface roughness of undeformed pack ice (e.g., from factors like location in the floe, direction of the relative current, season of the year) to successfully pursue this approach. This paper addresses specifically the question: What is the under-ice roughness, z_0, of a typical multiyear Arctic ice pack floe, separate from the effect of pressure ridge keels and sizable areas of first-year ice? This is not the same as determining the "aggregate" drag coefficient for the SHEBA region, but is instead the first

step in a systematic approach to including other ice types in such a determination.

[8] The research approach is as follows. Section 2 describes the experimental setup and measurements made at the main SHEBA turbulence mast during the yearlong project. In section 3, the ratio of mean current speed to friction velocity at the topmost instrument cluster on the SHEBA ocean turbulence mast is calculated for the entire project and used to derive simple drag coefficients and roughness length based on naive application of the law of the wall. Section 4 utilizes an IOBL turbulence model for estimates of surface stress and roughness, taking into account stress attenuation and buoyancy effects in the rotational boundary layer. One objective is to illustrate that horizontal heterogeneity in the ice undersurface often played a significant role in the turbulence structure. Section 5 develops an empirical method for estimating surface roughness assuming that even for the measurement level closest to the surface, turbulence scales are determined by the entire boundary layer turbulence structure, and are manifested in the local "mixing length." Mixing length is estimated from the peak wave number in the weighted vertical velocity power spectrum, and is combined with measured stress and mean velocity to estimate log z_0 by integrating the equation of motion. Discussion and summary follow in section 6.

2. Measurement Program and Data Analysis

[9] The oceanic program for SHEBA included deployment and maintenance of a mast suspended through an ice hydrohole with turbulence instrument clusters (TICs) at multiple levels in the ocean boundary layer. Each TIC comprises three small, partially ducted mechanical current meters mounted along mutually orthogonal axes canted approximately 45° with the horizontal (in order to measure small vertical velocities), mounted near fast response thermistors (Sea-Bird Electronics, SBE 03) and ducted conductivity meters (SBE 04). One cluster included an open electrode microstructure conductivity sensor (SBE 07). Data from the TICs feed to a highly modified SBE 9/11 CTD equipped with compass, pressure, and tilt sensors at a rate of six samples per second, recorded digitally. The rigid mast may be lowered by winch to arbitrary depths in the upper ocean. For SHEBA, it was held stationary most of the time. During the first half of the experiment (October 1997 to March 1998), there were four clusters mounted 4 m apart, with the uppermost cluster nominally 4 m below the ice/ocean interface.

[10] The mast was initially about 150 m north of the Canadian Coast Guard icebreaker *Des Grossiellier* that was moored to a large, multiyear ice floe to serve as the base for the SHEBA project. The mast was about 110 m west of a well defined, multiyear pressure ridge running north, which was oriented at approximately right angles to another pressure ridge system emanating westward from the bow of the ship. The latter became a zone of significant shear and alternating lead and pressure ridge formation later in the winter. When we deployed in early October 1997, the ice was intensively hummocked. We chose the thickest "undeformed" ice available for the turbulence mast hydrohole, which was nevertheless only about 2 m thick. In March 1998, ice deformation forced relocation of the oceanographic station to a new location several hundred meters northeast of the ship, in an area somewhat farther removed from any obvious pressure ridge features. The ice was again drilled repeatedly to find a remnant of a hummock from the previous summer (thickest undeformed ice), in anticipation of extensive summer melt pond formation. From the surface, there was no obvious difference between the two sites, except for the ship and pressure ridge systems described above, but in effect, the relocation provided two separate experiments for the main turbulence mast, each lasting for about half the total deployment. In expectation of increased biological fouling during summer (requiring frequent cleaning), the mast was redeployed at the end of March with two clusters instead of four, nominally at 4 and 8 m below the ice, later raised to 2 and 6 m at the end of June.

[11] The turbulence mast system (described in detail, e.g., by *McPhee* [1992, 1994] and *McPhee and Stanton* [1996]) is capable of measuring velocity and temperature fluctuations well into the inertial subrange. Turbulent fluxes are calculated using an advective transformation (Reynolds analogy) to estimate ensemble mean deviatory products from the zero-lag (in time) covariances. The method assumes a "spectral gap" between turbulent fluctuations and other time-varying phenomena. Experience has shown that "15-min realizations" usually separate the turbulence successfully, but it should be noted that much variability is expected from one realization to the next, because the timescale of energy containing eddies is often a sizable fraction of the 15-min averaging period.

[12] The turbulence mast operated continuously from 10 October 1997 until 28 September 1998, interrupted briefly by the forced relocation of the oceanographic measurement site in March 1998 and by occasional periods of intense biofouling in July 1998. The mechanical current meters have a finite velocity threshold, which combined with the orthogonal geometry of the cluster, dictates a practical lower velocity limit for valid three-dimensional currents measured relative to the drifting ice of around 5 cm s^{-1}. Early in the deployment, there were times when electronic noise from the nearby cycling CTD winch degraded temperature and conductivity signals in the upper two clusters, however this was fixed in early November 1998 (thanks to M. Golden and T. Lehman).

[13] The general analysis scheme was to treat each cluster separately, dividing its data record into 15-min realizations. Objective quality checks were performed on each segment: primarily that all three components turned consistently during the 15-min segment, plus absence of electronic noise and reasonable mean flow behavior. Acceptable segments were then rotated into a "streamline" coordinate system aligned with the mean flow velocity vector measured relative to the drifting ice, i.e., one in which $\langle v \rangle = \langle w \rangle = 0$, where angle brackets represent the 15-min average. Deviatory time series (T', S', u', v', w') were then formed from the five data streams, where, e.g., $T' = T - \langle T \rangle$, linearly detrended. Turbulent flux quantities were obtained from the average products of the deviatory time series:

$$\tau = \langle u'w' \rangle + i\langle v'w' \rangle$$
$$u_* = |\tau|^{1/2}$$
$$\langle w'T' \rangle$$
$$\langle w'S' \rangle$$

Note that Reynolds stress τ is a two-dimensional (complex) vector, and that the definition of friction velocity, u_*, is

local, vis-a-vis u_{*0}, which is friction velocity at the ice/ocean interface.

[14] In addition to mean and flux quantities, variance spectra were calculated for the deviatory time series. Spectral components were averaged in evenly spaced bins of log k, where k is the angular wave number, i.e., 2π times frequency divided by mean current speed, following the method described by *McPhee* [1994]. The vertical velocity variance spectrum provides two quantities to complement the direct flux measurements. First is the turbulent kinetic energy (TKE) dissipation rate ε, given by

$$\varepsilon^{2/3} = \frac{3}{4\alpha_\varepsilon} S_{ww}(k) k^{5/3} \tag{3}$$

where S_{ww} is the vertical velocity spectra energy density at wave number k in the inertial subrange ($-5/3$ log/log slope) of the spectrum, and α_ε is Kolmogorov's constant, taken to be 0.51 [*Hinze*, 1975; *McPhee*, 1994]. The second quantity is a length scale associated with the inverse of the wave number at the peak of the weighted (kS_{ww}) spectrum:

$$\lambda = c_\lambda / k_{\max} \tag{4}$$

where $c_\lambda = 0.85$. Earlier work [*McPhee and Martinson*, 1994; *McPhee*, 1994; *McPhee and Stanton*, 1996] showed empirically that λ is a good proxy for the mixing length, which is eddy viscosity divided by local friction velocity, i.e.,

$$K = u_* \lambda$$

[15] The automated technique for extracting these quantities from the spectra is illustrated for a segment of data representing the average of all 15-min realizations in a 6-h period centered at 0600 UT on 3 November 1997 (day 317.25). Vertical velocity spectra at four levels, averaged in equally spaced wave number bins (Figure 1a), are fitted with a high-order polynomial, which provides (1) $k_{\max}$, the wave number at the maximum in $k\,S_{ww}(k)$ (vertical dashed lines), and (2) the value of $k\,S_{ww}(k)$ where the negative slope of the polynomial function first exceeds two thirds (solid circles). Corresponding values for λ from equation (4) are shown in Figure 1b, along with a dashed line with slope $-\kappa$ representing the surface layer mixing length (section 3), originating at the ice undersurface at $z = -2.1$ m. The TKE dissipation rate from equation (3) is shown in Figure 1C. The calculation of ε is insensitive to the choice of abscissa provided the sample is taken in a region of the spectrum with the slope of the inertial subrange ($-2/3$ log/log slope in the weighted representation). For example, since the inertial subranges overlap for clusters 3 and 4, they have similar values for ε despite being sampled at different k values. In a steady, horizontally homogeneous flow where buoyancy flux and vertical transport of TKE are negligible, the equivalence of shear production and dissipation provides an estimate of local friction velocity [*McPhee*, 1994]: $u_{*\varepsilon} = (\lambda\varepsilon)^{1/3}$, as plotted in Figure 1D, along with the direct covariance estimates: $u_* = (\langle u'w' \rangle^2 + \langle v'w' \rangle^2)^{1/4}$, which are drawn with lines representing twice the sample standard deviation. While in this example the difference between the two estimates is not very significant, in general an imbalance between the two would suggest that other factors besides shear production and dissipation play a role in the TKE balance.

[16] Roughly 24,000 segments (6000 h) of ocean turbulence data distributed across all seasons passed quality screening. These were further bin averaged in 3-h or 6-h blocks for the entire project, depending on the applications described below.

[17] The TIC mast system provided a continuous record of pressure, which was calibrated periodically for atmospheric pressure adjustment. The dynamically important measurement, however, is vertical displacement from the ice undersurface, which varied with ice thickness. A time series of ice draft was estimated by averaging data from ice thickness gauges in the vicinity of the TIC mast with similar ice thickness (data courtesy of D. Perovich), using occasional tie points determined by measuring the distance from the water surface to the bottom of the TIC hydrohole.

3. Near Surface Stress and Current Velocity

[18] Fifteen-minute turbulent flow realizations meeting the minimum quality criteria were bin averaged in 3-h blocks for the uppermost cluster, TIC 1, when there were at least four samples in each period with mean Reynolds stress exceeding 10^{-5} m^2 s^{-2}. These data are summarized in Figure 2, showing the ratio U_{cl1}/u_{*cl1} for each 3-h average plus monthly mean values; and in Figure 3, with monthly mean values for valid three hour samples of current speed, drag coefficient, $c_{cl1} = (U_{cl1}/u_{*cl1})^{-2}$, and log z_0, calculated according to

$$\log z_0 = \log h_{cl1} - \kappa U_{cl1}/u_{*_{cl1}} \tag{5}$$

where h_{cl1} is the displacement of TIC 1 from the interface, and we have assumed neutral stability and no variation in stress from the interface to the measurement level.

[19] At first glance, there appears to be a seasonal aspect to the drag; however, excluding July when there were relatively few samples, the largest month-to-month change occurs from March to April, coinciding with relocation of the oceanographic site. As this is normally a time of year when one would expect fewest changes in the ice underside, the under-ice surface may just have been smoother near site 2. Yet there was evidence of unexpected basal melting from heat flux measurements and ice thickness gauges (D. Perovich, personal communication, 1998) in March 1998, which might have decreased ice roughness across the entire floe. On the other hand, if July is again excluded, there was a significant increase in drag from May to September, spanning the season of intense bottom melting. By September, the U_{cl1}/u_{*cl1} ratio and inferred drag characteristics are similar to site 1 values the previous winter.

[20] The weighted average values of log z_0 for sites 1 and 2 differ substantially, as indicated in Figure 3, implying overall roughness lengths of 1.2 and 0.3 cm for sites 1 and 2, respectively. The weighted average log z_0 over all months is -5.1, implying $\bar{z}_0 = 0.6$ cm based on direct application of the law of the wall to measurements at the uppermost TIC.

[21] In essence, the analysis in this section matches the sophistication of most previous determinations of drag characteristics for Arctic pack ice. Interestingly, Figure 3c shows monthly variation in z_0, as determined by naive

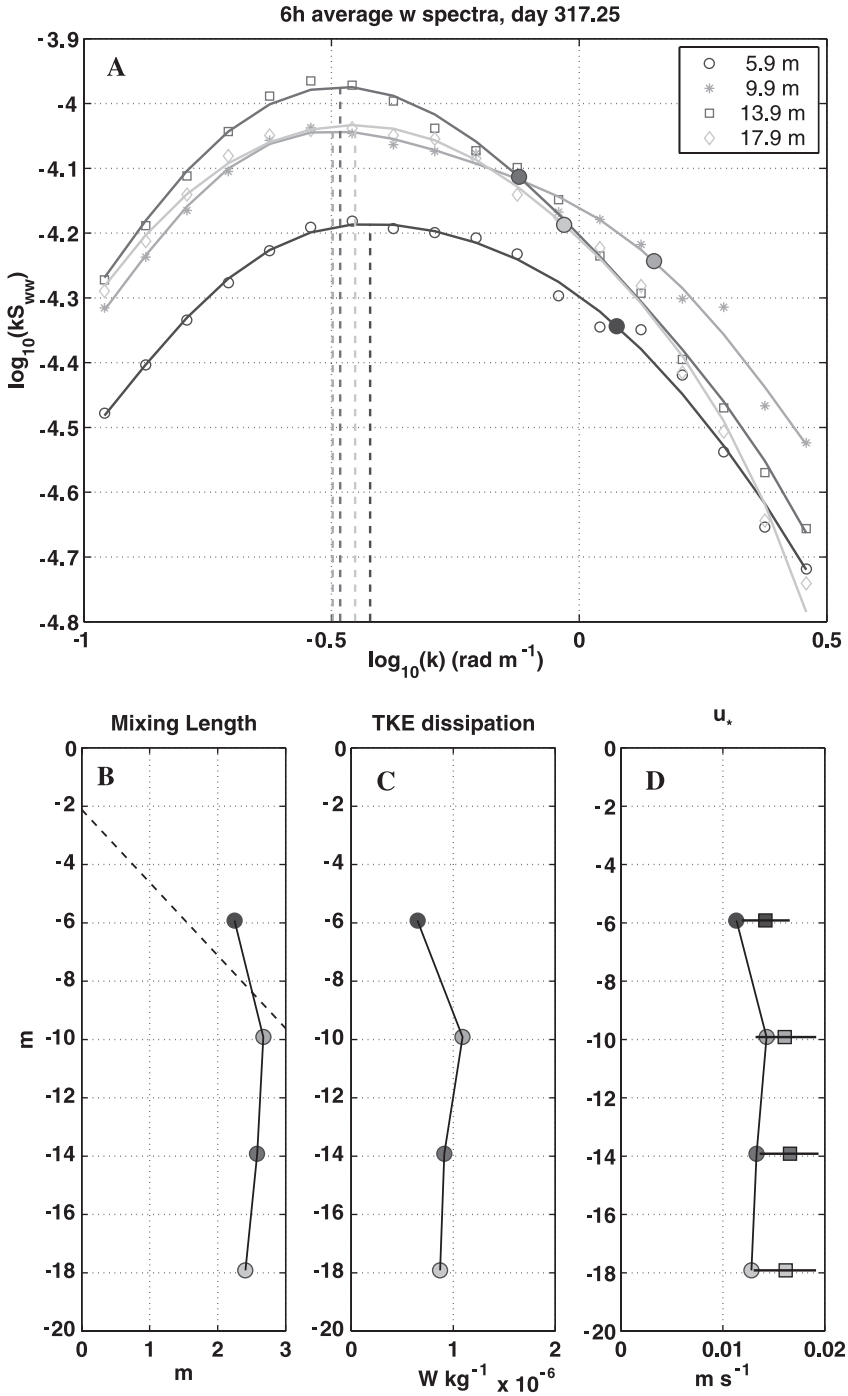

Figure 1. (a) Vertical velocity spectra averaged in evenly spaced logarithmic bins then fitted with a high-order polynomial. $\lambda = 0.85/k_{max}$ where k_{max} is the maximum in the fitted function, indicated by dashed lines. Dissipation is estimated from ordinates in the inertial subrange, indicated by solid circles. (b) Corresponding vertical distribution of λ. The dashed line is von Kàrmàn's constant times the distance from the ice/water interface. (c) Vertical distribution of ε. (d) Friction velocity determined from ε and λ (circles) and from average of square root of covariance Reynolds stress (squares). Bars represent twice the standard deviation of the 15-min samples.

application of the law of the wall equation (5) under one floe, that corresponds roughly with the range of roughness lengths reported in the literature, i.e., from a fraction of a millimeter to several centimeters. In terms of searching for a representative roughness length characteristic of undeformed multiyear ice, these results are thus not very helpful, e.g., there is a fourfold difference in z_0 between the two sites. The discussion in section 1 suggested that drag defined for an arbitrary level, as with c_1 above, could respond to a number of factors besides the physical roughness of the undersurface. Partly for heuristic reasons and partly to pursue the ''scaling up'' strategy described in

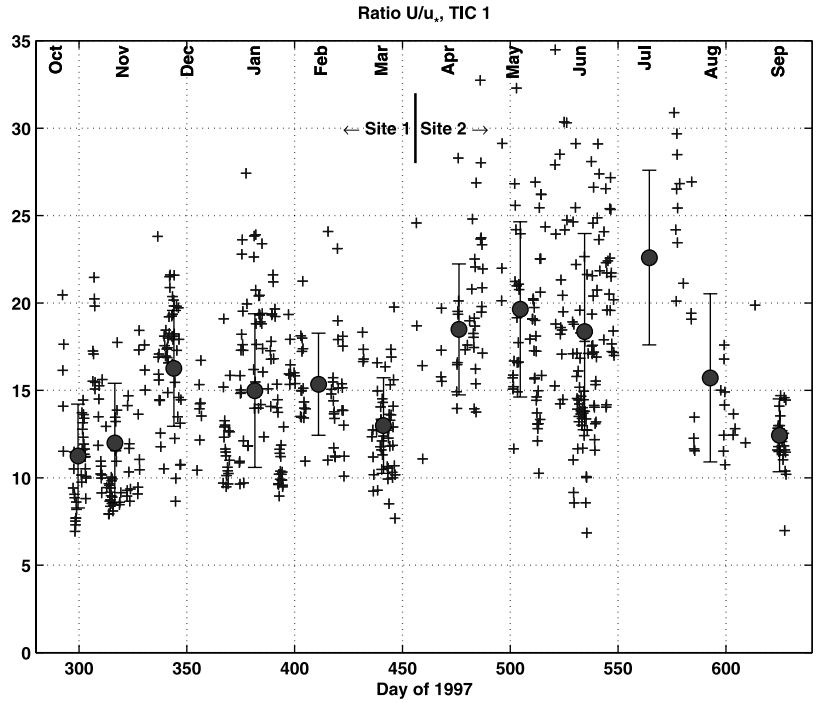

Figure 2. Current speed divided by friction speed from the uppermost TIC. Circles with standard deviation error bars are monthly averages. The project was split by relocation of the oceanography station in March 1998, as indicated by the line separating site 1 from site 2.

section 1, the z_0 question is approached from different perspectives in the remainder of the paper.

4. IOBL Modeling of Turbulent Stress and Surface Roughness

[22] Turbulent fluxes of momentum and scalar properties vary with depth in response to both rotational (Coriolis) and buoyancy (density gradient) forces. In summer for example, meltwater stratifies the water column, so that turbulent eddies must work against gravity as well as inertial forces. Reduced turbulence scales and eddy viscosity mean less drag, but not necessarily a smoother surface. IOBL stress is usually measured beyond the surface layer, and will in general be different from stress at the interface. Similarly, as distance increases, current shear loses its inverse z dependence, and rotation (angular shear) becomes important. Properly accounting for these factors requires a realistic IOBL model. This section first presents two examples of IOBL measurements compared with a numerical model, based on *local turbulence closure* (LTC) as described by *McPhee* [1999] and *McPhee et al.* [1999]. In both cases, current and Reynolds stress measured with TIC 1 are used to force the model, which then predicts the current structure and friction velocity throughout the remainder of the IOBL. In the first instance, the model provides a reasonable approximation to the observed Reynolds stress and mean flow shear (including turning). In the second case, the model does a poor job of simulating observed turbulent stress, which increases with depth.

[23] Application of the model throughout the entire project provides a second estimate of surface stress and z_0, one that includes buoyancy and rotation (but still assumes horizontal homogeneity).

[24] The LTC model assumes that turbulence is instantaneously in local equilibrium with forcing conditions, and steps iteratively through a series of steady state momentum equation solutions that incrementally adjust the eddy diffusivity profiles to prescribed temperature and salinity (density) profiles. The model is forced by a specified surface stress, with buoyancy flux at the ice/ocean interface calculated from ice growth rate, mainly a function of the interface enthalpy balance. An ice submodel calculates growth rate and buoyancy flux at the interface by balancing latent exchange with conductive heat flux in the ice less heat flux from the ocean, obtained with a bulk formula dependent on u_{*0} and temperature elevation from freezing [*McPhee*, 1992]. ''Percolation'' of fresh or brackish surface water can affect the surface buoyancy flux in the model but was not considered here. It may have been significant during one storm starting late in July 1998.

[25] Since stress is measured some distance from the interface, the model is iterated from an initial guess for u_{*0} until modeled stress matches observed at the uppermost cluster. For driving the model, and for the data/model comparisons, turbulence data from the uppermost TIC were averaged in 6-h blocks. Similarly, upper ocean temperature and salinity profiles from the cycling CTD (data courtesy of T. Stanton) were averaged in 1-m bins over the same 6-h intervals. Provided each 6-h average was obtained from at least ten 15-min turbulent flow realizations and at least four cycling CTD profiles, the LTC model was solved. Over the whole project, there were 229 6-h samples meeting these criteria, with the LTC model solved for each.

[26] Surface roughness is extracted from the model results and measured mean current speed at the upper TIC following the geometric construction developed by *McPhee et al.* [1999, Figure 2]. Let $\widehat{u}_s$, $\widehat{u}_1$, and $\widehat{u}_{cl}$ be velocities (in an

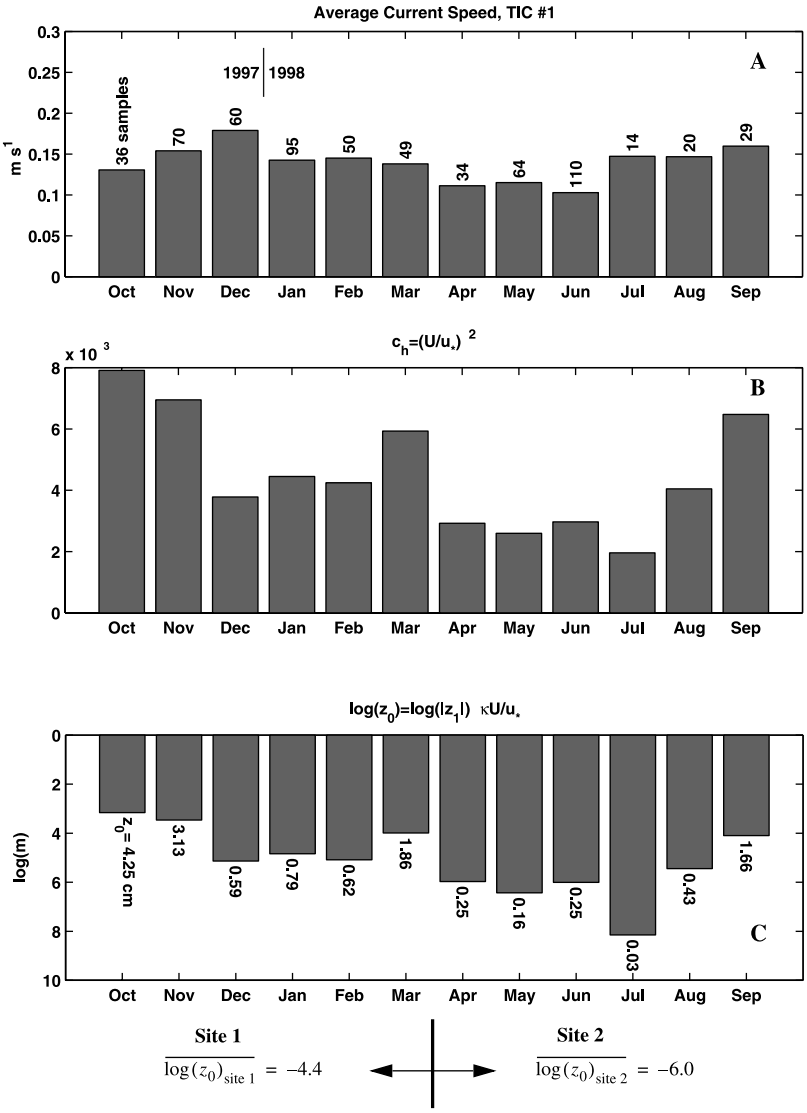

Figure 3. (a) Average current speed in each month for the samples used in Figure 2. (b) Monthly average value for c_h from the ratios in Figure 2. (c) log z_0 from the drag coefficients, where z_1 is the mean elevation of TIC 1 with respect to the ice/ocean interface. Mean values for sites 1 and 2 imply z_0 values of 0.012 and 0.003 m, respectively.

absolute reference frame) at the surface, at the uppermost grid point in the model, z_1, and at the cluster level, respectively. The last two are calculated by the model. The coordinate system is chosen so that the real (x) axis is aligned with surface stress, and the change in velocity from the surface to z_1 is $\delta u = \hat{u}_1 - \hat{u}_s$, which is real if $|z_1|$ is small. The relative velocity between the surface and the measurement level is then

$$\hat{u}_{\mathrm{rel}} = \hat{u}_1 - \hat{u}_{cl} + \delta u$$

whence

$$\delta\hat{u} = \left(S^2 - \mathrm{Im}(\hat{u}_1 - \hat{u}_{\mathrm{cl}})^2\right)^{1/2} - \mathrm{Re}\,(\hat{u}_1 - \hat{u}_{\mathrm{cl}})$$

where S is the measured current speed. Then the law of the wall applied to the uppermost grid point yields

$$\log z_0 = \log|z_1| - \frac{\kappa\delta u}{u_{*0}} \qquad (6)$$

The first grid point (z_1) is chosen close enough to the interface that equation (6) holds for all reasonable conditions.

[27] Two examples of model/data comparison are shown. Both had nearly identical average current speed at the uppermost cluster (0.187 and 0.184 m s^{-1}, respectively), but differed in Reynolds stress measured there by a factor of more than four. Case 1, with relatively low stress is shown in Figure 4. Temperature and salinity are prescribed in the model and used to adjust the mixing length and eddy viscosity iteratively. Salinity (Figure 4b), which controls density, shows a surprisingly shallow pycnocline for the date (25 January 1999), and also that there is stratification in the "mixing layer." The latter reduces maximum mixing length in the model, increasing stress attenuation with depth (Figure 4c). In general, the model reproduces the stress profile with reasonable accuracy. Note that interface friction velocity (u_{*0}) is about

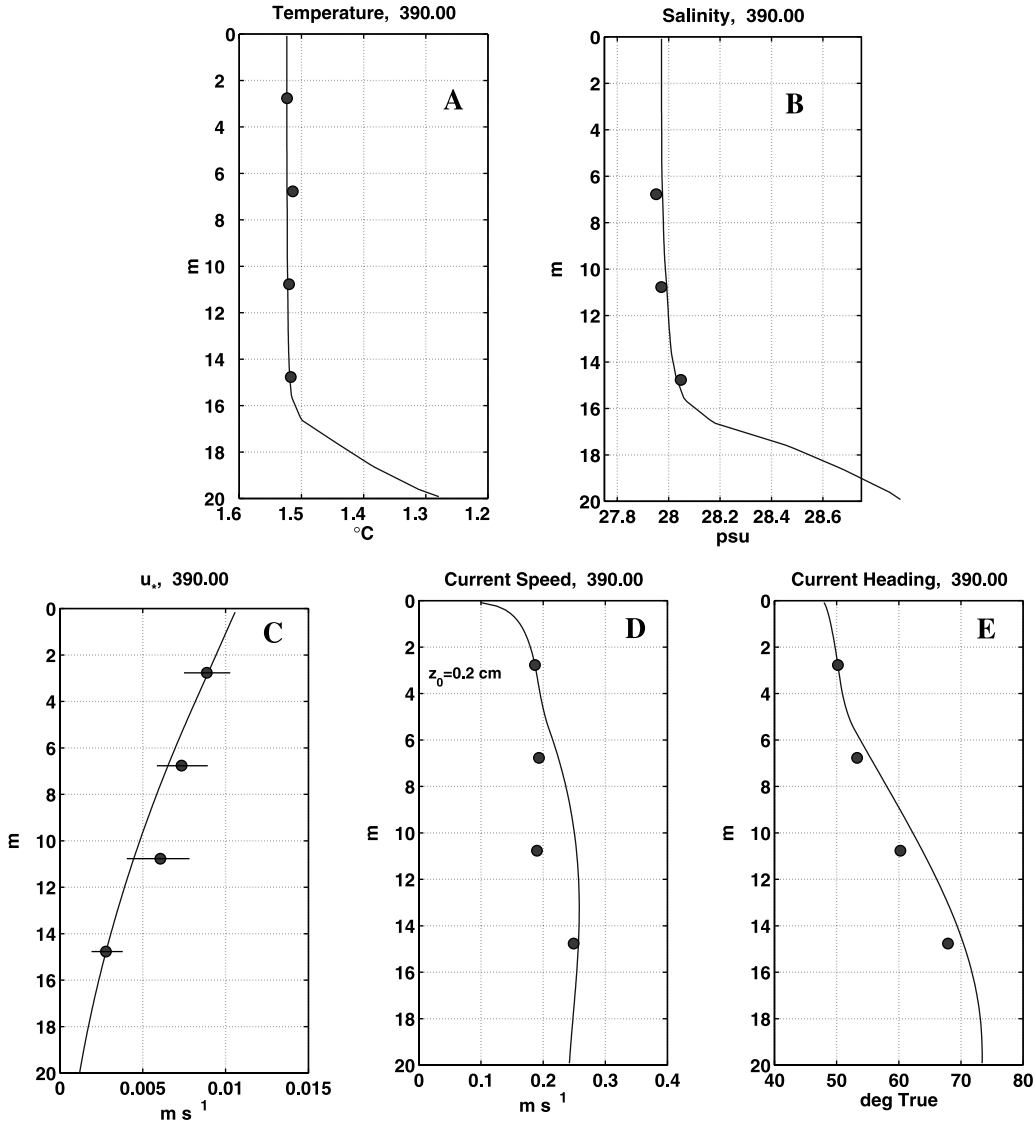

Figure 4. Model case 1. (a) Temperature measured with the SHEBA CTD profiler (solid curve), averaged for 6 h centered on day 390 (0000 UT, 25 January 1998), with TIC (turbulence mast) shown as solid circles. (b) Measured salinity. Note the slight negative gradient in the ''mixing layer.'' (c) Solid curve: modeled friction velocity (square root of Reynolds stress) from the IOBL model, forced by measured stress at TIC 1, and observed T/S profiles. Solid circles are measured values at each turbulence mast level, with bars indicating twice the sample standard deviation of all 15-min realizations in the 6-h average. (d) and (e) Current speed and direction in a reference frame fixed to the drifting ice; log z_0 is chosen to force the model to match observed velocity at TIC 1.

20% greater than at the first measurement level (surface stress about 0.1 Pa). The technique described above was used to estimate log z_0 from the mean velocity measured 2.8 m below the ice, from which a model velocity profile in a frame of reference drifting with the ice was constructed (Figures 4d and 4e). Although measured speed deviates somewhat from simulated at TICs 3 and 4, the angular shear (Ekman turning), with nearly 20° turning across the span of the instrument mast, is reasonably well simulated.

[28] Case 2 (Figure 5), from earlier in the drift (10 November 1997), provides a striking contrast. Despite similar current speeds, Reynolds stress at TIC 1 is much larger, implying modeled interface stress of about 0.5 Pa. Here the pycnocline is 8–9 m deeper, and salinity (density) is indeed well mixed over most of the mixing layer. Because of much larger stress and lack of stratification in the second simulation, average eddy viscosity in the mixing layer is more than ten times as large as in case 1. This is apparent in the decreased shear (speed and angular) in both model and measurements (Figures 5d and 5e). Note that a much larger surface roughness (~11 cm) is needed to reconcile u_{*0} and current speed at 3.8 m.

[29] The main feature of measured stress in case 2 is its increase with depth (Figure 5c). Measured Reynolds stress at TIC 3 is about 44% greater than at TIC 1, 8 m above. A

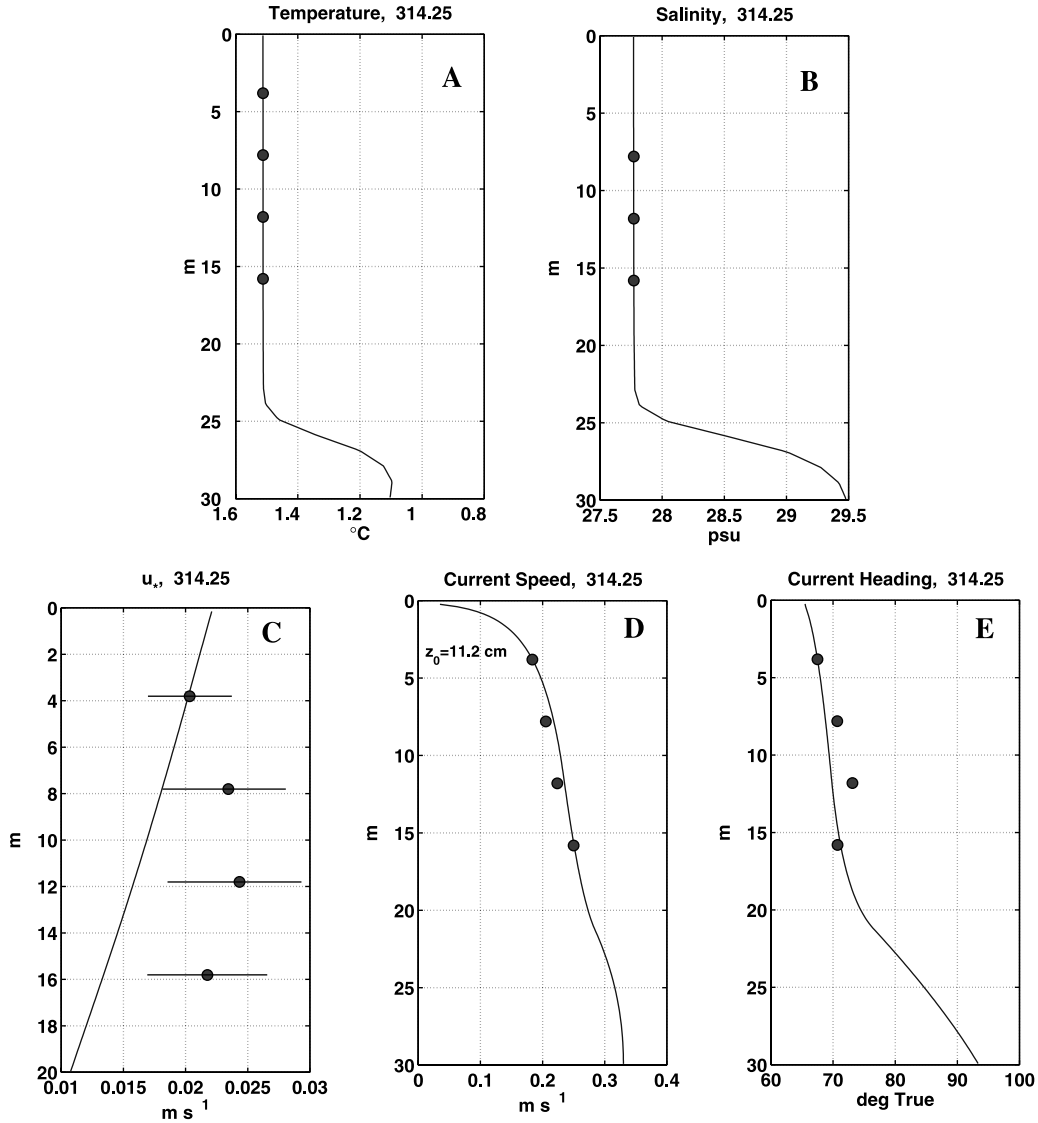

Figure 5. Same as Figure 4, except model case 2. Note that measured stress at TIC 1 is more than four times as large as for case 1, while current speed is similar. The model cannot simulate the increase in friction velocity with depth.

one-dimensional model that diffuses momentum away from the solid boundary cannot replicate this behavior, even if turbulence scales are enhanced by destabilizing surface buoyancy flux. The most likely source for increased velocity covariance at depth is horizontal diffusion away from an upstream source of the turbulence. A major factor in interpreting turbulence measurements in natural boundary layers is that the surface is rarely uniform far enough upstream for the assumption of horizontal homogeneity to hold through the entire boundary layer. A convenient rule-of-thumb for obtaining rough estimates of the distance upstream, X, for which surface characteristics affect turbulence at a particular depth, h, in a shear flow has been suggested by J. Morison (personal communication, 1996): $X/h \sim U/u_*$. This ratio is of order 15 (Figure 2) so, for example, at 8 m (TIC 2) one might expect direct impact of "upstream" flow obstacles within ~120 m. During 1997, the SHEBA drift was predominantly westward, so that flow often approached the turbulence mast from across an old pressure ridge initially about 110 m west of Site 1 (this varied as the floe rotated). We found that turbulent stress often increased with depth, and interpreted this as response to larger roughness elements within the increased fetch sensed by deeper instruments. For case 2, the relative current heading of 70° T indicates flow across the ridge keel. However, this was also the flow direction for the lower cluster in case 1 (Figure 4e). The large difference in IOBL response is presumably explained by the fact that between 10 November 1997 (314) and 25 January 1998 (390), *Des Grossiellier's* heading rotated by about 50° clockwise (as did the floe), creating different upstream conditions for each case. Unfortunately, we lacked resources to adequately map the ice undersurface and have no complete picture of under-ice morphology in the vicinity of the mast.

[30] Although not shown here, in both cases the modeled turbulent fluxes of scalar temperature and salinity, though

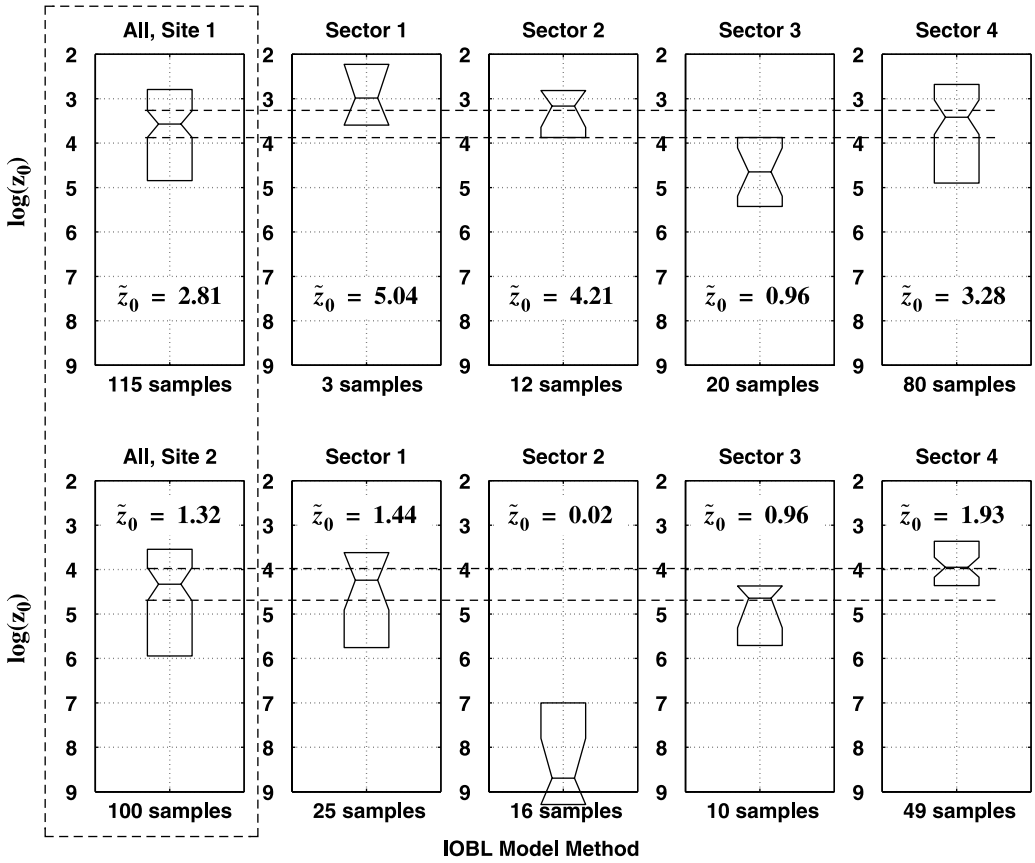

Figure 6. Schematic representation of the statistics of log z_0 for the IOBL model method, classified by site (rows) and sector from which the relative flow emanates. Notches represent a robust confidence interval for the median based on data sample quartiles. See text for details. Where notches overlap the dashed lines, median values are not significantly different from the total sample median. Roughness length (in cm) from the exponential of the median log z_0 value is shown in each box. Sector 1 is from the north (315° to 045°T), Sector 2 from east (045 to 135), Sector 3 from south (135 to 225), and Sector 4 from west (225 to 315).

small, compare reasonably well with measurements, indicating that the model eddy diffusivities are plausible.

[31] Surface roughness (i.e., log z_0) was calculated for each of the 229 6-h modeling runs described above. Results were classified according to site, and by mean current direction sector, where sector 1 indicates flow from the north in the quadrant from 315° to 045° T; sectors 2, 3, and 4 are from the east, south, and west, respectively. Statistics of log z_0 are summarized graphically in Figure 6. There were several samples for which conditions indicated that the surface was *hydraulically smooth*, meaning that z_0 only has meaning in terms of the local friction velocity and molecular viscosity, not the actual physical characteristics of the surface. These tend to make very small values for log z_0, with a potential for large first moment at one tail of the log z_0 probability distribution. In this case, the median is a more robust estimator of the central value [*Press et al.*, 1988], hence a method adapted from the MatLab Boxplot routine was chosen to display the results. For each panel, the lower and upper lines are the 25th and 75th percentiles of each sample set, with the intermediate line the median value (the listed value for each panel is $\tilde{z}_0$ =100exp(*median*(log z_0)), i.e., the surface roughness length in centimeters). Asymmetry in the boxes indicates skewness. Notches represent a robust confidence interval based on the quartile limits:

$$CI = q_{50\,\%} \pm \frac{1.57(q_{75\,\%} - q_{25\,\%})}{\sqrt{n}} \tag{7}$$

where q is the percentile level for the sample ($q_{50\%}$ is the median) of length n. Where notches overlap (extended from the total sample set for each site by the dashed lines), the statistical difference between the sample subset median and the total set median is not significant at the 95% confidence level.

[32] Figure 6 shows that for Site 1 (October 1997 to March 1998), 6-h samples meeting the quality criteria occurred mostly for flow from the west (80 samples) and south (20 samples). Thus the determination of the overall median value of log z_0 for Site 1 ($\tilde{z}_0$ = 2.8 cm) must have been heavily influenced by the pressure ridge keel initially west of the turbulence mast. Flow from sector 3 (south) produced a smaller value ($\tilde{z}_0$ = 1.0 cm) than from sector 4 ($\tilde{z}_0$ = 3.3 cm). According to the IOBL calculations, median log z_0 at site 2 is significantly smaller than at site 1, implying

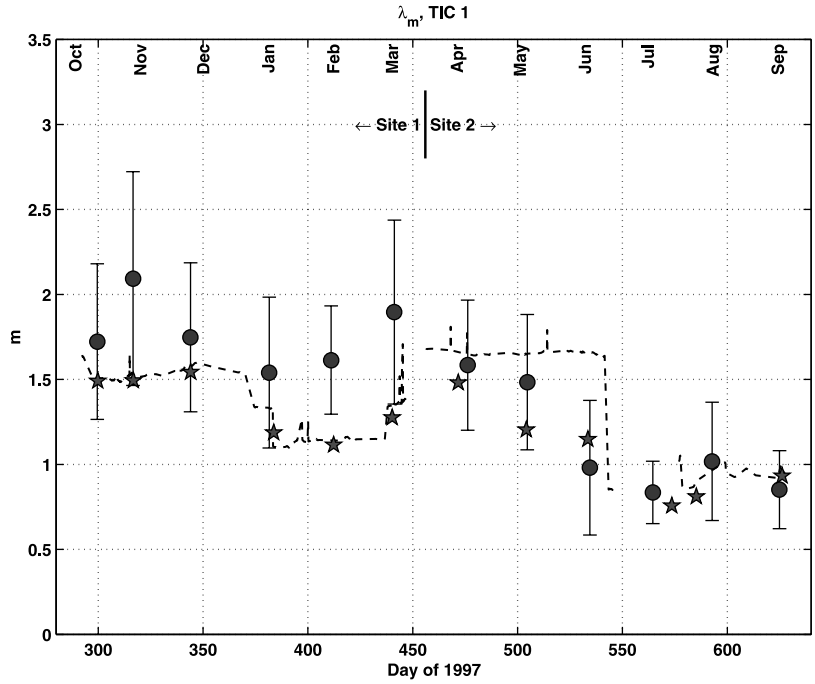

Figure 7. Monthly average mixing length determined from spectral peak wavenumbers for each 3-h sample from cluster 1 (solid circles). Error bars represent twice the sample standard deviation. The dashed line is von Kàrmàn's constant times the displacement of TIC 1 from the ice underside. Pentagrams are monthly averages of modeled mixing length evaluated at the TIC 1 depth.

$\tilde{z}_0 = 1.3$ cm there. At site 2, only flow from the east (sector 2) stands out as significantly different from other directions, and is so small as to suggest that the surface in that direction may often have appeared hydraulically smooth.

[33] Compared with the logarithmic surface layer estimates of section 3, surface roughness obtained from the IOBL model is larger at both sites (2.8 versus 1.2 cm at site 1; 1.3 versus 0.3 cm at site 2), but the increase is much greater at site 2. The overall increase results from higher interface stress estimates as the model adjusts for stress attenuation with depth. The greater increase at site 2 results from both buoyancy effects in the model, which are important during summer, and decreased surface stress, which moves TIC 1 farther away from the surface layer in a similarity sense.

5. An Ad Hoc Method Based on Mixing Length

[34] The model of section 4 serves the important function of adjusting turbulence measurements at or beyond the outer edge of the surface layer for both depth and buoyancy, but it does not adequately describe relatively frequent situations where stress was observed to *increase* with depth as in Figure 5. It seems likely that in those cases, more intense turbulence in the deeper part of the boundary layer would influence turbulence scales close to the surface and change the shear/stress relationship. In this section, we use another flow parameter described in section 2, namely mixing length λ, to explore this possibility. Monthly averages of λ based on spectral peaks as described in section 2 are shown in Figure 7 as circles with standard deviation error bars. These were obtained from spectra averaged in 3-h bins as in Figure 2. Also plotted are the surface layer mixing length, $\kappa|z|$ at TIC 1 depth (dashed curve) and the mixing length at the same depth as calculated by averaging the IOBL model runs of section 4 (pentagrams). During the first half of the project, the model and surface layer values agree well, but the "measured" mixing length is often significantly larger. This means first that interfacial stress was large enough that TIC 1 was usually in the depth range where modeled λ increases linearly; and second, that the turbulence scale indicated by eddy size at the w spectral peak was consistently larger than modeled. In other words, turbulent energy and scales at the TIC 1 level were being enhanced either by buoyancy flux (from freezing) or from some other source, such as diffusion of TKE upward from below. Based on average growth rates of thicker ice at SHEBA, destabilizing buoyancy flux was typically too small to have much impact on IOBL dynamics. At site 2, spectral mixing length was on average closer to the modeled value, and both were often less than $\kappa|z_m|$, particularly during the April–June quarter when TIC 1 was nominally 4 m below the ice. In the model this results both from lower interfacial stress, and from stratification of the water column.

[35] In general, if the method used for calculating z_0 consistently underestimates mixing length, roughness length will be overestimated, and vice versa. A simple illustration is provided by considering a constant stress layer with mixing length increasing linearly from the surface to an arbitrary value λ_h at z_h, where here we use the convention that the z coordinate increases positively away from the surface. The integral of $\tau = KU_z$ is then

$$\log z_0 = \log z_h - \frac{\lambda_h U}{z_h u_{*0}} \tag{8}$$

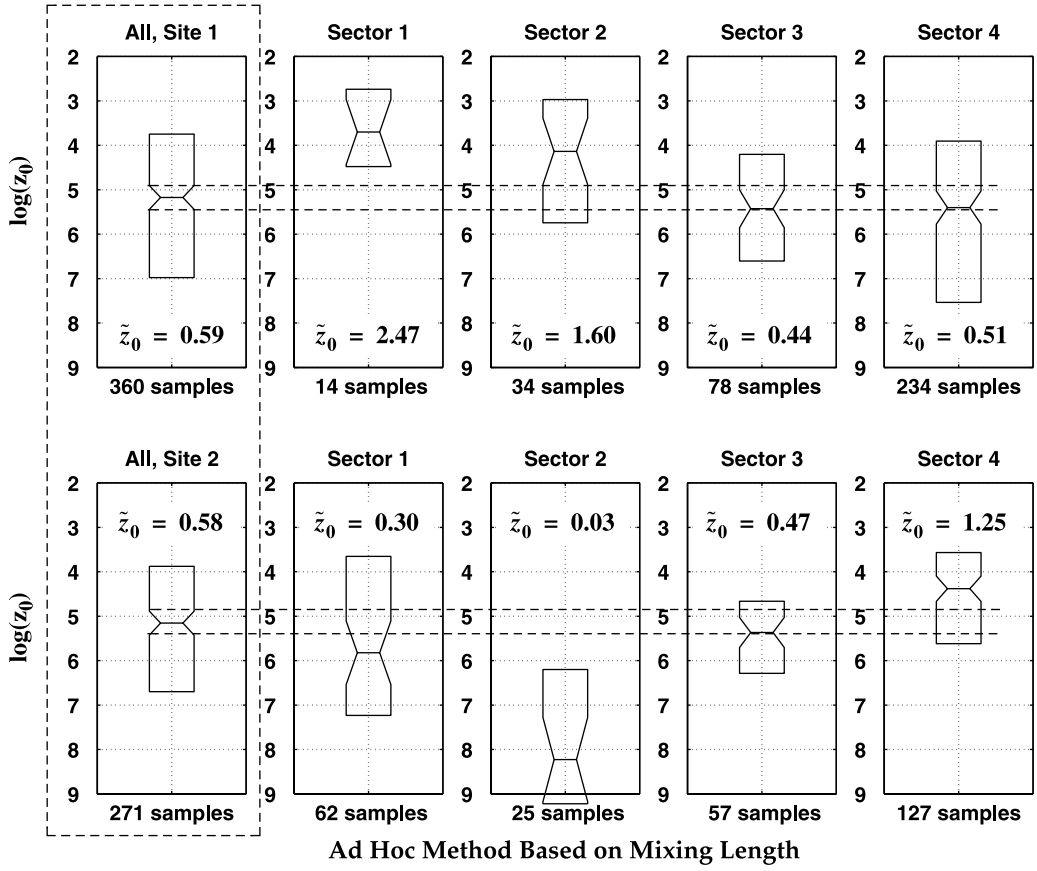

Figure 8. As in Figure 6, except log z_0 determined by the ad hoc mixing length method.

If $\lambda_h > \kappa z_h$, surface roughness is smaller than calculated by equation (5).

[36] Treating λ_m as an independently measured variable suggests a phenomenological method for estimating surface roughness using measured stress (τ), current speed (U), and mixing length (λ_m) at the level of the uppermost cluster, z_m. It was developed under the following assumptions:

[37] (1) Reynolds stress magnitude varies linearly from its surface value to near zero at the base of the mixed layer, h_{ml}. For small values of z/h_{ml}, friction velocity is approximated by the first two terms of a Taylor series expansion:

$$u_* = \tau^{1/2} \cong u_{*0}\left(1 - \frac{z}{2h_{m1}}\right)$$

[38] (2) If $\lambda_m/\kappa > z_m$, assume that λ varies linearly: $\lambda = \frac{\lambda_m}{z_m} z$, so that

$$U = \frac{u_{*0} z_m}{\lambda_m} \int_{z_0}^{z_m} \left(\frac{1}{z} - 1\right) dz$$

For $z_0 \ll z_m$, the integral yields

$$\log z_0 = \log z_m - \frac{z_m}{2h_{m1}} - \frac{\lambda_m U_m}{z_m u_{*0}} \tag{9}$$

[39] (3) Conversely, if $\lambda_m/\kappa \leq z_m$, then

$$\lambda_m = \begin{cases} \kappa z & z \leq \lambda_m/\kappa \\ \lambda_m & \lambda_m/\kappa < z \leq z_m \end{cases}$$

i.e., assume the measurement distance exceeds the extent of the surface layer ($z_{sl} \leq \lambda_m/\kappa$). Current velocity at z_{sl} is then

$$U_{sl} = U_m - \lambda_m u_{*0}\left(z_m - \frac{\lambda_m}{\kappa}\right)\left(1 - \frac{1}{2h_{ml}}\right) \tag{10}$$

and the law of the wall (equation (5), modified for slight variation in u_*) then furnishes

$$\log z_0 = \log \frac{\lambda_m}{\kappa} - \frac{\lambda_m}{2\kappa h_{ml}} - \frac{\kappa U_{sl}}{u_{*0}} \tag{11}$$

[40] Statistics of z_0 calculated using the mixing length (λ) method (equation (9) or equations (10) and (11)) are summarized in Figure 8. The interesting result is that by this analysis, the two sites have nearly identical overall roughness lengths (0.6 cm) based on median values of log z_0. Only two sectors, north at site 1 (rough), east at site 2 (smooth), lie convincingly outside the confidence interval for the totals samples. Both are derived from relatively few samples.

[41] Seasonal dependence was tested by grouping the z_0 determinations (λ method) into quarters (Figure 9). As with the site dependence, no convincing seasonal difference emerges. The median value of log z_0 for the period from

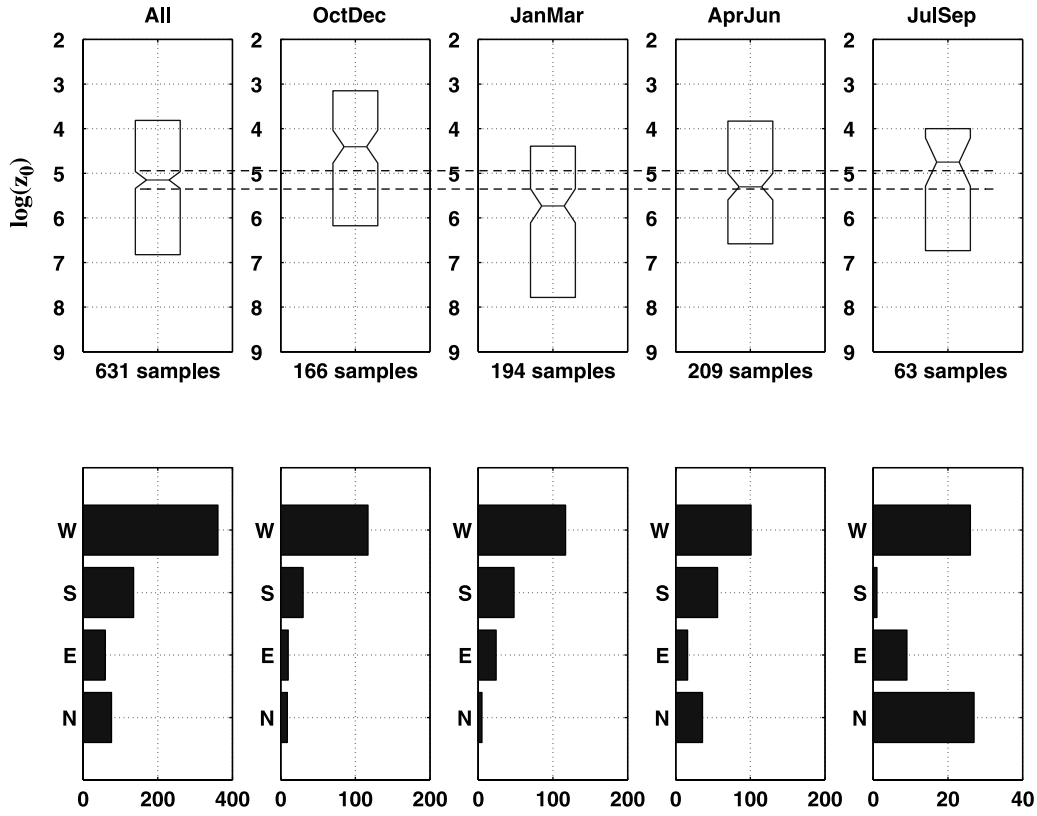

Figure 9. Distributions of log z_0 for the mixing length method for all 3-h samples and by quarterly distribution (upper row). Sample histograms by flow sector (bottom row).

October to December is larger than the overall median, and the value for January to March smaller, though with only marginal statistical significance. With the exception of flow from the west at site 2, which comprised about 9% of the samples there, the mixing length method provides a surprisingly uniform picture of under-ice roughness.

6. Discussion and Conclusions

[42] Two models were developed to estimate bottom surface roughness length of the undeformed SHEBA floe. The first solves a horizontally homogeneous boundary layer model to determine surface conditions from turbulent stress and current speed measured at the uppermost instrument cluster, 2 to 4 m from the ice/ocean interface. The second is empirically based, using mixing length determined from vertical velocity spectra the TIC 1 level, then used to integrate the momentum equation to the surface. Statistics of log z_0 as computed by the IOBL and λ methods are summarized in Figure 10. Numbers under each panel represent the range of z_0 associated with the 95% confidence interval for the median of log z_0. Both methods may be compared with naive application of the law of the wall equation (5) as summarized in Figure 3. It is interesting that the overall mean value for equation (5) matches the "λ-derived" median value closely, but an important distinction is that the latter analysis shows no significant difference between the two sites and little seasonal dependence, whereas the former shows much variability.

[43] Which is appropriate? The IOBL model was introduced to estimate the effects of rotation and buoyancy on the boundary layer between the surface and the first cluster. Its impact is obvious at site 2, where Reynolds stress at TIC 1 was on average considerably lower than at site 1. The model both increases the interface friction velocity and decreases the mean eddy diffusivity when the model surface layer depth (determined dynamically from u_{*0} and $\langle w'b' \rangle_0$) is less than the measurement distance, compared with the law-of-the-wall calculation. The net result is to increase z_0, compared with equation (5). However, failure of the horizontally homogeneous model to account for persistent increase in Reynolds stress with depth during the first half of the drift prompted development of the mixing length (λ) method. This shifts determination of eddy viscosity between the interface and measurement level from a theoretical or modeling exercise, to an empirical procedure based on the inverse wave number at the peak in the turbulent vertical velocity spectrum. There is little precedence for this approach, but the results appear reasonably robust, and indicate that in general the roughness of the SHEBA floe was remarkably uniform, with little positional, directional, or seasonal variation. The only glaring exception was flow from the east at site 2, comprising only about 4% of the total number of samples. There was large sample-to-sample variability, yet when integrated over time at a particular location, equivalent to averaging over the area of a floe at a particular time, the λ method suggests a fairly high degree of uniformity.

[44] It is interesting to compare the present results with selected previous determinations. The first estimate of under-ice z_0 was made from 16 mean current profiles under sea ice near Ice Station Arlis II, east of Greenland in 1965 [*Untersteiner and Badgley*, 1965]. As reanalyzed by *Ling and Untersteiner* [1974], their data yielded a 90% confidence

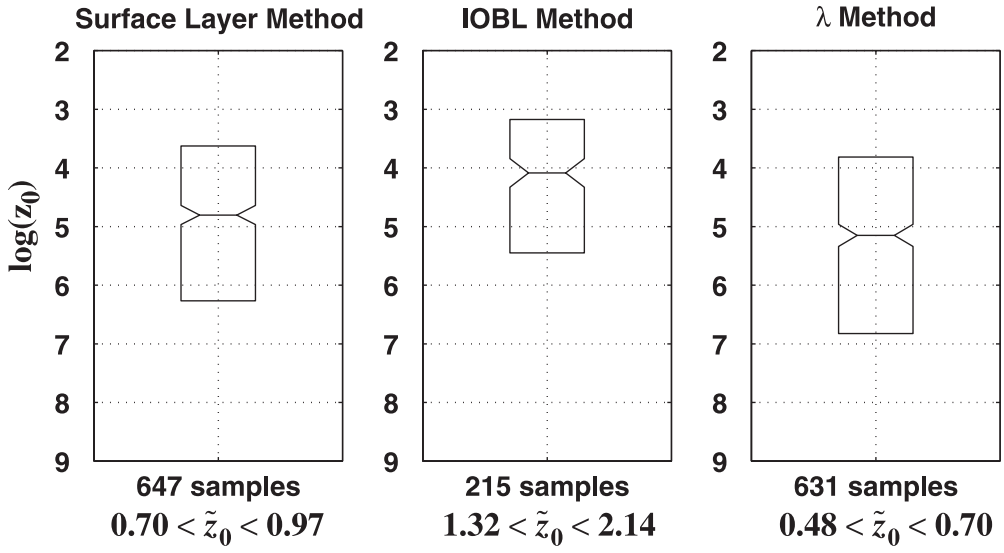

Figure 10. Comparison of statistical distributions for the two models used in determining log z_0. Confidence intervals for the median value of log z_0 (notches) converted to roughness length ranges in centimeters are listed below each box.

interval 0.82 cm < z_0 < 1.93 cm. This overlaps with the IOBL method here, but is slightly larger than the median value determined by the λ method. On the other hand, analysis of summer data from the AIDJEX stations in 1975 implied a value for the z_0 of around 10 cm [*McPhee*, 1979], based on the free-drift force balance as discussed in section 1.

[45] For a larger scale view of the differences between AIDJEX and SHEBA, a comparison of the ratio between ice drift speed and wind speed is instructive. The rule of thumb is that for free-drift conditions (meaning that internal ice stress gradients are not important in the force balance), Arctic pack ice drifts at about 2% of the speed of the surface (10 m) wind. For AIDJEX, the ratio between ice speed and wind speed, V_{ice}/W_{10}, was calculated every 12 h from smoothed wind and ice drift velocities (for $W_{10} > 2.5$ m s^{-1}) at the four stations, then averaged in 20-day blocks (see *McPhee* [1980, Table 1]). Similarly, the ratios of 3-h averages of ice speed (with the inertial component removed) and 10-m wind speed (data courtesy of the SHEBA Project Office) were grouped into 20-day blocks for the SHEBA drift and averaged. The two time series were adjusted to a common day-of-year time base as plotted in Figure 11a. It appears that SHEBA encountered considerably less resistance from internal ice stress gradients than did the AIDJEX stations, consistent with thinner ice and different drift patterns.

[46] As a check on the magnitude of z_0 as calculated by the λ method, I inverted the free-drift stress calculation to use measured ice velocity and wind speed, along with the Rossby similarity estimate of ice/ocean stress via equation (1), to "back out" estimates of the 10-m wind drag coefficient. Assuming (somewhat arbitrarily) that periods for which the ice/wind drift ratio exceeded 1.8% were predominantly periods of free drift, one can estimate the wind drag coefficient from the steady force balance

$$\rho_a c_{10} W_{10}^2 = |\rho u_{*0} \boldsymbol{u}_{*0} + \rho_i h_i f \boldsymbol{V}_i| \qquad (12)$$

where ρ_a and ρ_I are air and ice densities, respectively and the complex vector quantities $\boldsymbol{u}_{*0}$ and $\boldsymbol{V}_i$ are related by equation (1) with z_0 = 0.0058 m. Results are shown in Figure 11b. There appears to be some indication of a seasonal change, with higher c_{10} in the summer and lower in winter, consistent with seasonal changes in atmospheric stratification. However, it should be noted that the two high values in summer could also be an artifact of assuming neutral stratification in the ocean by holding A and B constant in equation (1). The mean value for c_{10} derived from the force balance, about 0.0018, is close to the "very smooth" multiyear ice classification suggested by *Guest and Davidson* [1991, Table 1], but is at the high end of the range reported for SHEBA by *Andreas et al.* [2001].

[47] It should be emphasized again that the z_0 value being discussed in this paper is that which pertains to the "undeformed" SHEBA multiyear floe. The purpose in developing the λ method was to remove the apparent effect of pressure ridge keels some distance upstream from the turbulence mast in order to estimate roughness in the immediate vicinity of the mast. To move to a regional value that would be truly appropriate for the above exercise (and for SHEBA goals discussed in section 1), requires consideration of the added drag from isolated pressure keels and floe edges, along with reduced drag from smoother, newly frozen ice and open water. The best estimate of under-ice surface roughness for a "typical" multiyear floe in the SHEBA vicinity, namely 0.0048 < $\tilde{z}_0$ < 0.007 m (Figure 10), appears to be fairly robust in terms of location on the floe, direction of relative current, and season of the year. It thus provides an important basis to which modifications imposed by other ice types, and by variable temperature/salinity conditions in the upper ocean, can be added. Research is currently underway to combine IOP measurements with more sophisticated multidimensional and large eddy simulation modeling, in order to better characterize the drag and associated roughness length for ridged and smooth ice types.

[48] **Acknowledgments.** This work was supported by the National Science Foundation grants OPP9701558, OPP9725478, OPP0084275, and OPP0084269 and by the Office of Naval Research grant N00014-96-C-

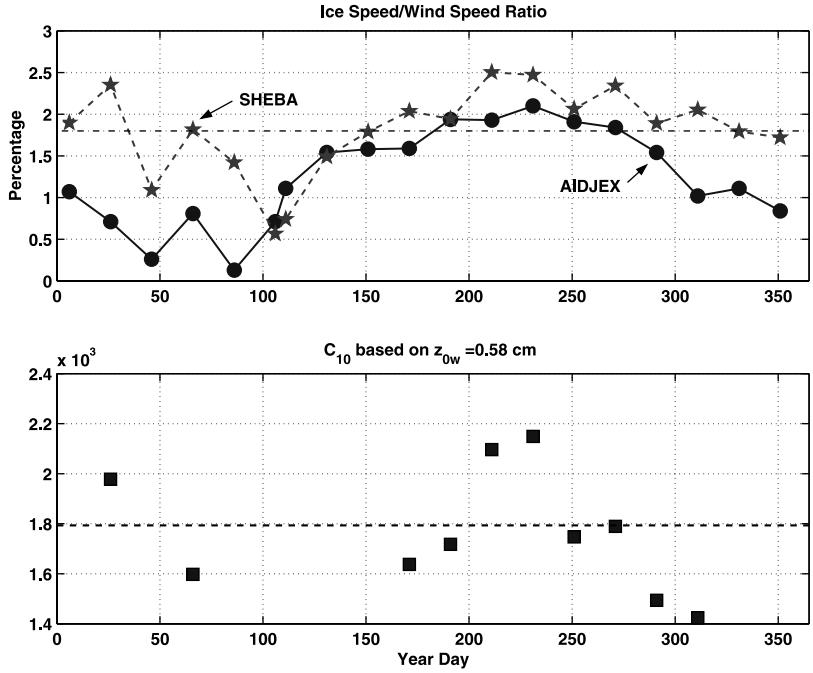

Figure 11. (a) Ratio of ice speed to near surface wind speed for the AIDJEX stations (circles) and SHEBA (pentagrams) averaged in 20-day blocks (AIDJEX data from *McPhee* [1980]). Inertial components have been removed from the SHEBA ice velocity, determined by complex demodulation of global positioning system data. Ten-meter wind data courtesy of the SHEBA Project Office. (b) Ten-meter wind drag coefficient determined from the ice velocity and wind velocity using the Rossby similarity law for 20-day segments when the ice speed to wind speed ratio exceeded 1.8%.

0032. Direct assistance in the field program by T. Lehman, J. Ardai, R. Andersen, B. Tremblay, S. Peacock, and J. Yazici was critical to success of the SHEBA ocean turbulence program, as was excellent support from the officers and crew of the CCGS *Des Grossiellier* and from the University of Washington Polar Science Center logistics staff.

References

Andreas, E. L., C. W. Fairall, P. S. Guest, and P. O. G. Persson, The air-ice drag coefficient measured for a year over Arctic sea ice, in *Proceedings of the Sixth Conference on Polar Meteorology and Oceanography, 14–18 May 2001, San Diego*, pp. 300–303, Am. Meteorol. Soc., Boston, Mass., 2001.

Blackadar, A. K., and H. Tennekes, Asymptotic similarity in neutral planetary boundary layers, *J. Atmos. Sci.*, *25*, 1015–1019, 1968.

Carsey, F. D., The boundary layer height in air stress measurements, in *Sea Ice Processes and Models*, edited by R. Pritchard, pp. 443–451, Univ. of Wash. Press, Seattle, 1980.

Crawford, G., L. Padman, and M. McPhee, Turbulent mixing in Barrow Strait, *Cont. Shelf Res.*, *19*, 205–245, 1999.

Guest, P. S., and K. L. Davidson, The aerodynamic roughness of different types of sea ice, *J. Geophys. Res.*, *96*, 4709–4721, 1991.

Hibler, W. D., III, A dynamic thermodynamic sea ice model, *J. Phys. Oceanogr.*, *10*, 815–846, 1980.

Hinze, J. O., *Turbulence*, 2nd ed., 790 pp., McGraw-Hill, New York, 1975.

Lemke, P., W. B. Owens, and W. D. Hibler III, A coupled sea ice-mixed layer-pycnocline model for the Weddell Sea, *J. Geophys. Res.*, *95*, 9513–9525, 1990.

Ling, C.-H., and N. Untersteiner, On the calculation of the roughness parameter of sea ice, *J. Geophys. Res.*, *79*, 4112–4114, 1974.

McPhee, M. G., The effect of the oceanic boundary layer on the mean drift of sea ice: Application of a simple model, *J. Phys. Oceanogr.*, *9*, 388–400, 1979.

McPhee, M. G., An analysis of pack ice drift in summer, in *Sea Ice Processes and Models*, edited by R. Pritchard, pp. 62–75, Univ. of Wash. Press, Seattle, 1980.

McPhee, M. G., Small scale processes, in *Polar Oceanography*, edited by W. Smith, pp. 287–334, Academic, San Diego, Calif., 1990.

McPhee, M. G., Turbulent heat flux in the upper ocean under sea ice, *J. Geophys. Res.*, *97*, 5365–5379, 1992.

McPhee, M. G., On the turbulent mixing length in the oceanic boundary layer, *J. Phys. Oceanogr.*, *24*, 2014–2031, 1994.

McPhee, M. G., Scales of turbulence and parameterization of mixing in the ocean boundary layer, *J. Mar. Syst.*, *21*, 55–65, 1999.

McPhee, M. G., and D. G. Martinson, Turbulent mixing under drifting pack ice in the Weddell Sea, *Science*, *263*, 218–221, 1994.

McPhee, M. G., and J. D. Smith, Measurements of the turbulent boundary layer under pack ice, *J. Phys. Oceanogr.*, *6*, 696–711, 1976.

McPhee, M. G., and T. P. Stanton, Turbulence in the statically unstable oceanic boundary layer under Arctic leads, *J. Geophys. Res.*, *101*, 6409–6428, 1996.

McPhee, M. G., G. A. Maykut, and J. H. Morison, Dynamics and thermodynamics of the ice/upper ocean system in the marginal ice zone of the Greenland Sea, *J. Geophys. Res.*, *92*, 7017–7031, 1987.

McPhee, M. G., C. Kottmeier, and J. H. Morison, Ocean heat flux in the central Weddell Sea in winter, *J. Phys. Oceanogr.*, *29*, 1166–1179, 1999.

Obukhov, A. M., Turbulence in an atmosphere with a non-uniform temperature (English translation), *Boundary Layer Meteorol.*, *2*, 7–29, 1971.

Pease, C. H., S. A. Salo, and J. E. Overland, Drag measurements for first-year sea ice over a shallow sea, *J. Geophys. Res.*, *88*, 2853–2862, 1983.

Press, W. H., B. P. Flannery, S. A. Teukolsky, and W. T. Vetterling, *Numerical Recipes in C, The Art of Scientific Computing*, 735 pp., Cambridge Univ. Press, New York, 1988.

Shirasawa, K., Water stress and ocean current measurements under first-year sea ice in the Canadian Arctic, *J. Geophys. Res.*, *91*, 14,305–14,314, 1986.

Stössel, A., Sensitivity of Southern Ocean sea-ice simulations to different atmospheric forcing algorithms, *Tellus*, *44A*, 395–413, 1992.

Untersteiner, N., and F. I. Badgley, The roughness parameters of sea ice, *J. Geophys. Res.*, *70*, 4573–4577, 1965.

M. G. McPhee, McPhee Research Company, 450 Clover Springs Road, Naches, WA 98937, USA. (mmcphee@starband.net)